RESEARCH ARTICLE

Anatomically induced changes in rice leaf mesophyll conductance explain the variation in photosynthetic nitrogen use efficiency under contrasting nitrogen supply

Limin Gao, Zhifeng Lu, Lei Ding, Kailiu Xie, Min Wang, Ning Ling and Shiwei Guo[*]

Abstract

Background: The ratio of CO_2 mesophyll conductance (g_m) to Ribulose-1, 5-bisphosphate carboxylase/oxygenase (Rubisco) content has been suggested to positively affect photosynthetic nitrogen use efficiency (PNUE). The anatomical basis of g_m has been quantified, but information on the relationship between cell-level anatomies and PNUE is less advanced. Here, hydroponic experiments were conducted in rice plants supplied with ammonium (NH_4^+) and nitrate (NO_3^-) under three N levels (low, 0.71 mM; intermediate, 2.86 mM; high, 7.14 mM) to investigate the gas exchange parameters, leaf anatomical structure and PNUE.

Results: The results showed a lower PNUE in plants supplied with high nitrogen and NH_4^+, which was positively correlated with the g_m/Rubisco ratio. A one-dimensional within-leaf model revealed that the resistance to CO_2 diffusion in the liquid phase (r_{liq}) dominated the overall mesophyll resistance (r_m), in which CO_2 transfer resistance in the cell wall, cytoplasm and stroma were significantly affected by nitrogen supply. The chloroplast surface area exposed to intercellular space (S_c) per Rubisco rather than the g_m/S_c ratio was positively correlated with PNUE and was thus considered a key component influencing PNUE.

Conclusion: In conclusion, our study emphasized that S_c was the most important anatomical trait in coordinating g_m and PNUE with contrasting N supply.

Keywords: Leaf anatomies, NH_4^+, NO_3^-, Mesophyll conductance, PNUE, Rubisco

* Correspondence: sguo@njau.edu.cn
Jiangsu Provincial Key Lab for Organic Solid Waste Utilization, National
Engineering Research Center for Organic-based Fertilizers, Jiangsu
Collaborative Innovation Center for Solid Organic Waste Resource Utilization,
Nanjing Agricultural University, Weigang 1, Nanjing 210095, China

Gao *et al. BMC Plant Biology* (2020) 20:527

Page 2 of 12

Background

Photosynthetic nitrogen use efficiency (PNUE), determined as the ratio of photosynthesis rate (P_n) to leaf organic nitrogen content [1], is a key component of nitrogen use efficiency (NUE) and an indicator of the relationship between leaf nitrogen (N) and P_n. Under the present atmosphere, the unsaturated CO_2 concentration in C3 leaves influences the carboxylation of Ribulose-1,5-disphosphate (RuBP) and results in a finite P_n, which fails to match the increase in leaf N and induces a decrease in PNUE [2]. By using an "evolutionary" algorithm, the partitioning of photosynthetic enzymes was altered based on a fixed total amount of protein-nitrogen for maximizing P_n, and the result showed that an increase in Ribulose-1, 5-bisphosphate carboxylase/oxygenase (Rubisco) was required to maximize P_n [3]. It was also well documented that higher leaf N allocation into Rubisco was linked with an enhancement in PNUE [4].

Numerous studies have clarified that the enhancement in Rubisco activity is another favorable candidate for improving RuBP carboxylation efficiency and P_n because of its poor catalytic ability under ambient conditions due to the low CO_2 concentration and the low affinity for CO_2 [1, 5]. As the substrate of Rubisco, CO_2 concentration in the chloroplast (C_c), which is determined by stomatal conductance (g_s) and mesophyll conductance (g_m), plays a dominant role in regulating Rubisco activity [6, 7]. It has been demonstrated that g_m induces 40% of the total decrease in CO_2 concentration between the atmosphere and the carboxylation sites of Rubisco [8]. In a previous study, Li et al. [5] argued that an increase in g_m was not sufficient to meet the carboxylation demand of the increased Rubisco content and eventually resulted in a decreased PNUE. Therefore, it is speculated that factors affecting g_m would influence Rubisco activity and the relationship between P_n and leaf N content.

Evidence is now mounting that g_m is largely dependent on leaf anatomical characteristics, including leaf thickness, cell wall thickness and chloroplast morphology [9, 10]. Higher leaf density and thicker mesophyll cell walls contribute to a reduction in g_m [9, 11–14], and mesophyll and/or chloroplast surface areas exposed to the intercellular space, S_{mes} and S_c, respectively, are positively correlated with g_m [15]. The overall importance of different anatomical traits in the restriction of g_m varies [16]. For gymnosperms, the strongest sources of g_m are cell wall and chloroplast thickness, variation in chloroplast shape and size, and S_c [9]. In lycophytes and bryophytes, the highest CO_2 diffusive resistance is mainly driven by extremely high cell wall thickness and low S_c [17]. Even though the anatomical factors influencing g_m have been widely studied, the role of these anatomical factors in influencing PNUE and their relative contribution in rice plants are still largely unknown.

Leaf anatomy is remarkably influenced by N nutrition; for example, decreasing leaf thickness and smaller chloroplasts with no starch granules have been detected in nitrogen-deficient leaves, while high-N leaves have more large chloroplasts with well-developed grana, stroma lamellae and starch granules per mesophyll cell [5, 18–20]. For different nitrogen forms, increased leaf thickness and a doubling of chloroplast volume with a larger internal membrane length have been found in NH_4^+-fed plants compared with NO_3^--fed plants [21–23]. In this study, we examine the responses of leaf anatomical characteristics, including leaf thickness, mesophyll cell size, chloroplast length and thickness, chloroplast number per mesophyll cell under NH_4^+ and NO_3^- nutrition with different N levels; moreover, we discuss the implications for understanding leaf trait variation with changes in N nutrition along the PNUE. Our objectives of the present study were as follows: (1) to identify the response of PNUE and leaf anatomical traits upon NH_4^+ and NO_3^- nutrition at different N levels; (2) to clarify the role of leaf anatomical factors in coordinating the g_m and PNUE under NH_4^+ and NO_3^- nutrition supply; and (3) to investigate the most limiting fraction of leaf anatomy in determining PNUE under different N supply.

Results

Effects of nitrogen supply on rice photosynthetic nitrogen use efficiency (PNUE)

Compared with those with low nitrogen supply (LAN and LNN), rice biomass and leaf area with intermediate and high nitrogen supply increased by 70–73% and 33–42% under NH_4^+ nutrition and by 30–48% and 40–41% under NO_3^- nutrition, respectively (Table 1). There were no significant differences in rice biomass and leaf area between the intermediate and high nitrogen supply conditions. Rice biomass was less affected by nitrogen forms at the same nitrogen level, while for intermediate nitrogen supply, the leaf area was decreased by 10% in NO_3^--fed plants than in NH_4^+-fed plants (Table 1). The leaf N content (N_L) was 54–62% and 66–80% higher under intermediate N supply and high N supply than under low N supply and was decreased by 9–11% under NO_3^- nutrition compared with that under NH_4^+ nutrition (Table 1). The Rubisco content was 26, 21 and 21% lower under low NO_3^- (LNN), intermediate NO_3^- (MNN) and high NO_3^- (HNN) than that under low NH_4^+ (LAN), intermediate NH_4^+ (MAN) and high NH_4^+ (HAN), respectively (Table 1). The stomatal conductance (g_s) was less affected by N supply than mesophyll conductance (g_m), which was increased by 72 and 24% in HAN and HNN, respectively, compared with that in LAN and LNN and decreased by 4–30% under NO_3^- compared to NH_4^+ nutrition (Table 1). Neither nitrogen supply levels nor nitrogen forms affected the chloroplast CO_2 concentration (C_c). With increasing leaf N content, the light-saturated photosynthetic rate (P_n) increased, while the photosynthetic nitrogen use efficiency (PNUE)

Gao *et al. BMC Plant Biology*   (2020) 20:527

Page 3 of 12

Table 1 Effects of different nitrogen supply levels on rice biomass (g), leaf area (cm^2), leaf nitrogen content (N_L, g m^{-2}), Rubisco content (g m^{-2}), stomatal conductance (g_s, mol CO_2 m^{-2} s^{-1}), mesophyll conductance (g_m, mol CO_2 m^{-2} s^{-1}), chloroplast CO_2 concentration (C_c, μmol mol^{-1}), photosynthesis rate (P_n, μmol m^{-2} s^{-1}), and photosynthetic nitrogen use efficiency (PNUE, μmol CO_2 $mmol^{-1}$ N s^{-1}). Rice plants ("Zhendao 11") were supplied with NH_4^+ (AN) or NO_3^- (NN) under 3 different amounts, low N (0.71 mM, LAN and LNN), intermediate N (2.86 mM, MAN and MNN), and high N (7.14 mM, HAN and HNN). Data are presented as the means ± SD of four replications. Significant differences ($P < 0.05$) between treatments are indicated by different letters

Treatments	Biomass	Area	N_L	Rubisco	g_s	g_m	C_c	P_n	PNUE
LAN	3.29 b	658 c	1.55 d	2.02 d	0.35 b	0.16 c	180 ab	24.61 b	0.22 b
MAN	5.71 a	932 a	2.38 b	3.16 b	0.45 a	0.24 ab	171 ab	28.74 a	0.17 cd
HAN	5.59 a	873 ab	2.58 a	3.67 a	0.49 a	0.28 a	187 a	29.25 a	0.16 d
LNN	3.77 b	595 c	1.30 e	1.49 e	0.27 b	0.16 c	165 b	25.00 b	0.27 a
MNN	4.92 a	837 b	2.11 c	2.50 c	0.44 a	0.20 bc	176 ab	29.86 a	0.20 bc
HNN	5.57 a	834 b	2.34 b	2.90 b	0.44 a	0.19 bc	176 ab	30.30 a	0.18 cd

decreased (Table 1, Fig. 1a, b). The PNUE was 21, 17 and 14% higher in LNN, MNN and HNN than in LAN, MAN and HAN, respectively (Table 1). Positive correlations existed between PNUE and both the C_c/Rubisco ratio and the g_m/Rubisco ratio (Fig. 1c, d).

Effects of nitrogen supply on leaf anatomical properties

With increasing leaf N supply levels, leaf thickness (T_L) and mesophyll cell thickness (T_m) increased in NH_4^+-fed plants but decreased in NO_3^--fed plants (Supplementary Fig. S1, Fig. 2a, b). Leaf dry mass per area (M_A), leaf density (D_L) and mesophyll cell wall thickness (T_{mc}) were increased by high N supply either with NH_4^+ or NO_3^-, and were lower under NO_3^- nutrition than under NH_4^+ nutrition. Mesophyll surface area exposed to intercellular airspace (S_{mes}) and the chloroplast surface area facing intercellular airspace (S_c) were upregulated significantly by increasing the nitrogen supply level (Fig. 2b). The S_{mes} increased by 22–37 and 21% under intermediate and high N supply conditions in NH_4^+ and NO_3^- nutrition, respectively, and the corresponding S_c increased by 22–38% and 21–24%, both compared with their respective low N supply conditions. No obvious differences in S_c between NH_4^+ and NO_3^- under low N levels were observed, but the S_c decreased by 11 and 20% under MNN and HNN, respectively, compared to that under MAN and HAN (Fig. 2b).

We further analyzed the chloroplast number per mesophyll cell (N_c), chloroplast length (L_c), chloroplast thickness (T_c), chloroplast surface area (Sur_c), chloroplast volume (Vol_c) and chloroplast section area (Sec_c). L_c was lower in NO_3^--fed plants than in NH_4^+-fed plants under intermediate and high N levels (Supplementary Fig. S1, Fig. 2c). Compared with that in LAN and LNN, the T_c was increased by 13–27% in MAN and HAN and 23–29% in MNN and HNN (Supplementary Fig. S1, Fig. 2c). Higher Sur_c and Vol_c were observed under high N supply. The chloroplast size was decreased under NO_3^- nutrition by 10–22%, 15–33%, and 10–40% in Sur_c, Vol_c

and Sec_c under low N, intermediate N and high N supply, respectively (Supplementary Fig. S1, Fig. 2d).
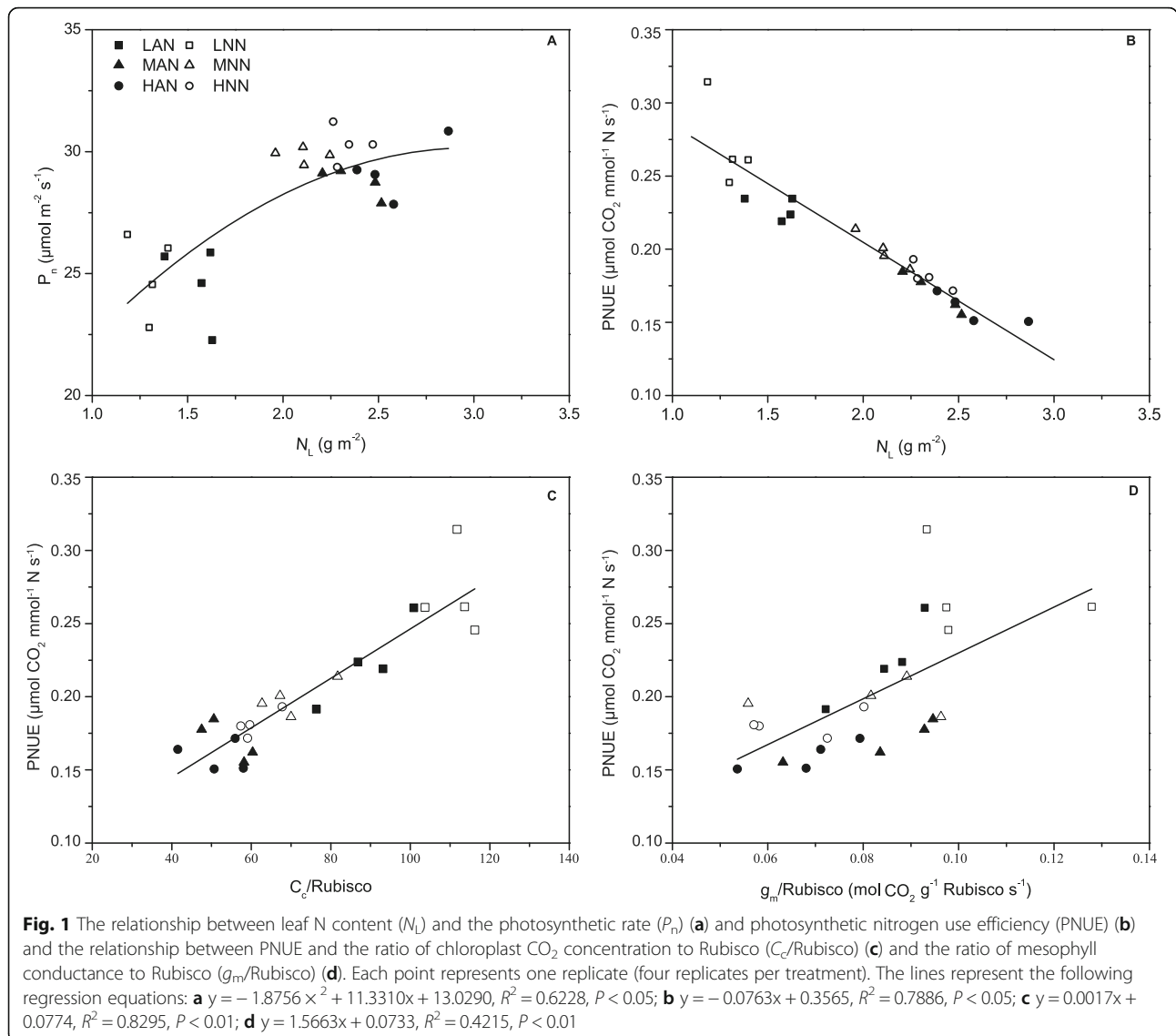
Anatomical limitations of mesophyll conductance

The values of g_m calculated according to the methods of Harley et al. [24] and Tomas et al. [16] were strongly positively linearly correlated (Supplementary Fig. S2, R^2 = 0.936). Further quantitative analysis showed that both the resistance in the gas phase (r_{ias}) and proportion of gas-phase limitations (l_{ias}) of g_m had little impact on the overall mesophyll resistance (Fig. 3), and that the liquid phase resistance (r_{liq}) was responsible for the limited g_m majority, among which stroma played a dominant role. High N supply significantly increased the resistance in the cell wall (r_{cw}) and stroma (r_{st}); compared with low N supply, g_m limited by the stroma (l_{st}) was increased by 9–10% under moderate N supply and by 9–13% under high N supply (Fig. 3b). Consistent with the absolute cytoplasm resistance, g_m limited by the cytoplasm (l_{cyt}) and cell wall (l_{cw}) were downregulated under high N supply and NO_3^- nutrition, respectively (Fig. 3). Among all the components, r_{cw} was the primary component affected by N forms and was 19, 23 and 16% higher under NH_4^+ nutrition than under NO_3^- nutrition in low N, intermediate N and high N supply, respectively (Fig. 3a).

Discussion

Effects of N supply on the g_m/Rubisco ratio and photosynthetic nitrogen use efficiency (PNUE)

Decreased PNUE under high N supply has been reported in previous and present studies (Table 1, Fig. 1) [5, 25–27]; referring to N forms, higher PNUE under NO_3^- nutrition than NH_4^+ nutrition in the present study is consistent with results in barley (*Hordeum vulgare* L.) [28], pine [29], and cucumber [30]. Leaf nitrogen allocation is an important factor influencing PNUE. Onoda et al. [31] indicated that a higher fraction of photosynthetic nitrogen in electron transport and Rubisco would contribute to increased PNUE in leaves with lower dry mass per area (M_A), while in leaves
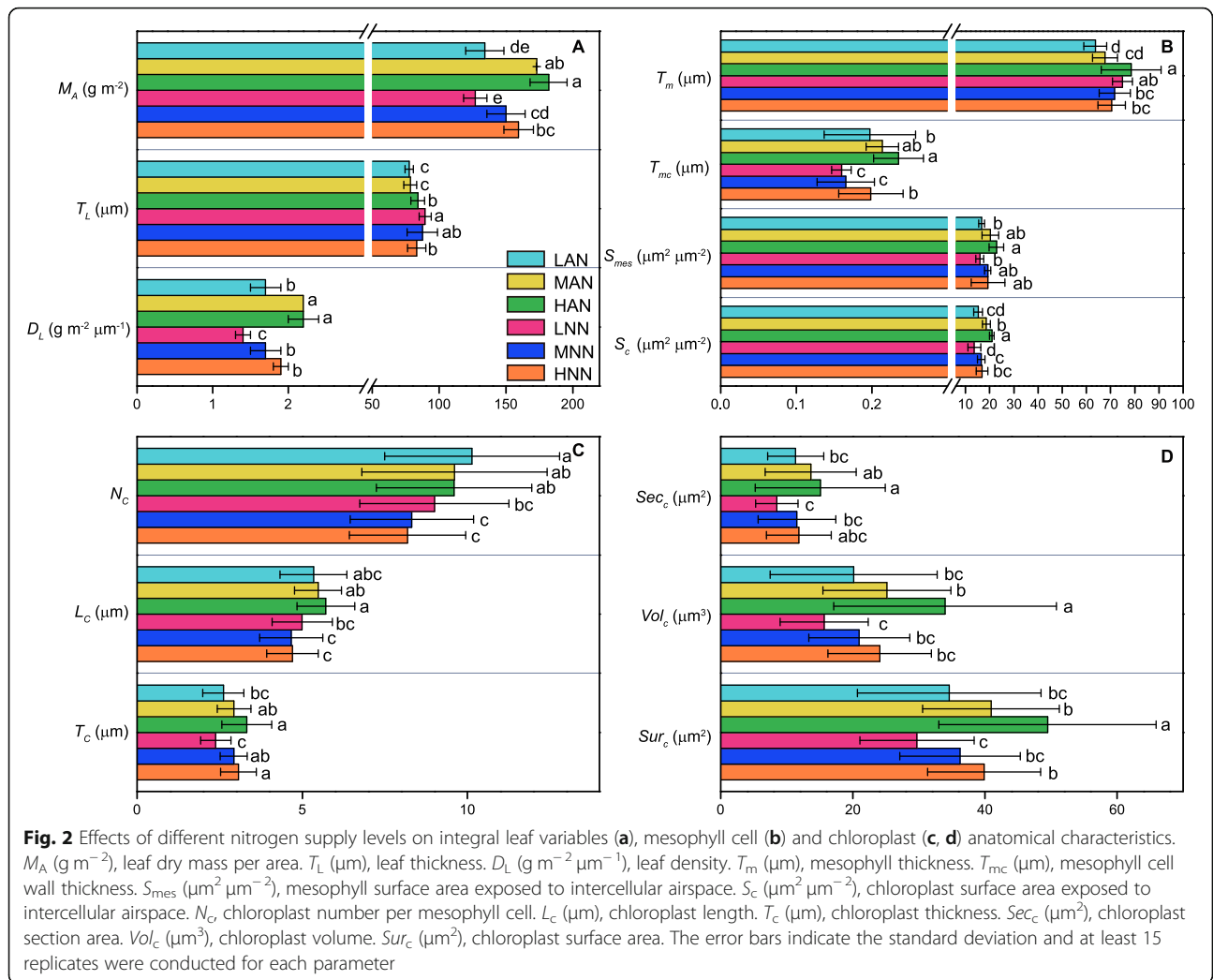
Fig. 1 The relationship between leaf N content (N_L) and the photosynthetic rate (P_n) (**a**) and photosynthetic nitrogen use efficiency (PNUE) (**b**) and the relationship between PNUE and the ratio of chloroplast CO_2 concentration to Rubisco (C_c/Rubisco) (**c**) and the ratio of mesophyll conductance to Rubisco (g_m/Rubisco) (**d**). Each point represents one replicate (four replicates per treatment). The lines represent the following regression equations: **a** $y = -1.8756 \times^2 + 11.3310x + 13.0290$, $R^2 = 0.6228$, $P < 0.05$; **b** $y = -0.0763x + 0.3565$, $R^2 = 0.7886$, $P < 0.05$; **c** $y = 0.0017x + 0.0774$, $R^2 = 0.8295$, $P < 0.01$; **d** $y = 1.5663x + 0.0733$, $R^2 = 0.4215$, $P < 0.01$

with higher M_A, the over-investment of nitrogen in photosynthetic nitrogen and/or cell walls would reduce PNUE [1]. The effect of the proportion of Rubisco in leaf N content on PNUE can be expressed based on Eq. (6):

$$\text{PNUE} = \frac{g_m}{\text{Rubisco}}(C_i - C_c)\frac{\text{Rubisco}}{N_L} \qquad (1)$$

Our study detected that the Rubisco allocation ratio was increased under high nitrogen supply but decreased under NO_3^- nutrition compared with NH_4^+ nutrition; however, the portion of Rubisco in leaf N content was not associated with PNUE (Fig. 4a). These results implied that Rubisco activity, rather than its content, played a dominant role in regulating PNUE [1, 5, 32].

An increased Rubisco allocation ratio requires increased CO_2 partial pressure at the carboxylation site (C_c) to meet carboxylation demands; however, the extent of the increase in C_c was less than that in Rubisco content, which resulted from the finite stomatal conductance (g_s) and mesophyll conductance (g_m). Li et al. [5] demonstrated that the smaller increases in g_m relative to Rubisco content resulted in relatively lower CO_2 levels in chloroplasts and PNUE (Fig. 1c, d), which implied that the g_m/Rubisco ratio rather than the absolute value of g_m was the key factor that regulates PNUE. We further compared the gap between estimated g_m and C_c proposed by Harley et al. [24] (Eq. 5, 6) and theoretical C_c ($C_{c\text{-Theoretical}}$) and g_m ($g_{m\text{-Theoretical}}$), which were calculated as follows based on Ding et al. [27], to evaluate the equilibrium state of g_m and Rubisco under different N nutrition conditions:

Fig. 2 Effects of different nitrogen supply levels on integral leaf variables (**a**), mesophyll cell (**b**) and chloroplast (**c**, **d**) anatomical characteristics. M_A (g m^{-2}), leaf dry mass per area. T_L (μm), leaf thickness. D_L (g m^{-2} μm^{-1}), leaf density. T_m (μm), mesophyll thickness. T_{mc} (μm), mesophyll cell wall thickness. S_{mes} (μm^2 μm^{-2}), mesophyll surface area exposed to intercellular airspace. S_c (μm^2 μm^{-2}), chloroplast surface area exposed to intercellular airspace. N_c, chloroplast number per mesophyll cell. L_c (μm), chloroplast length. T_c (μm), chloroplast thickness. Sec_c (μm^2), chloroplast section area. Vol_c (μm^3), chloroplast volume. Sur_c (μm^2), chloroplast surface area. The error bars indicate the standard deviation and at least 15 replicates were conducted for each parameter

$$g_m - \text{Theoretical (intermediate or high N)}$$
$$= \text{Rubisco (intermediate or high N)}$$
$$\times \frac{g_m}{\text{Rubisco}} \text{(low N)}$$

(2)
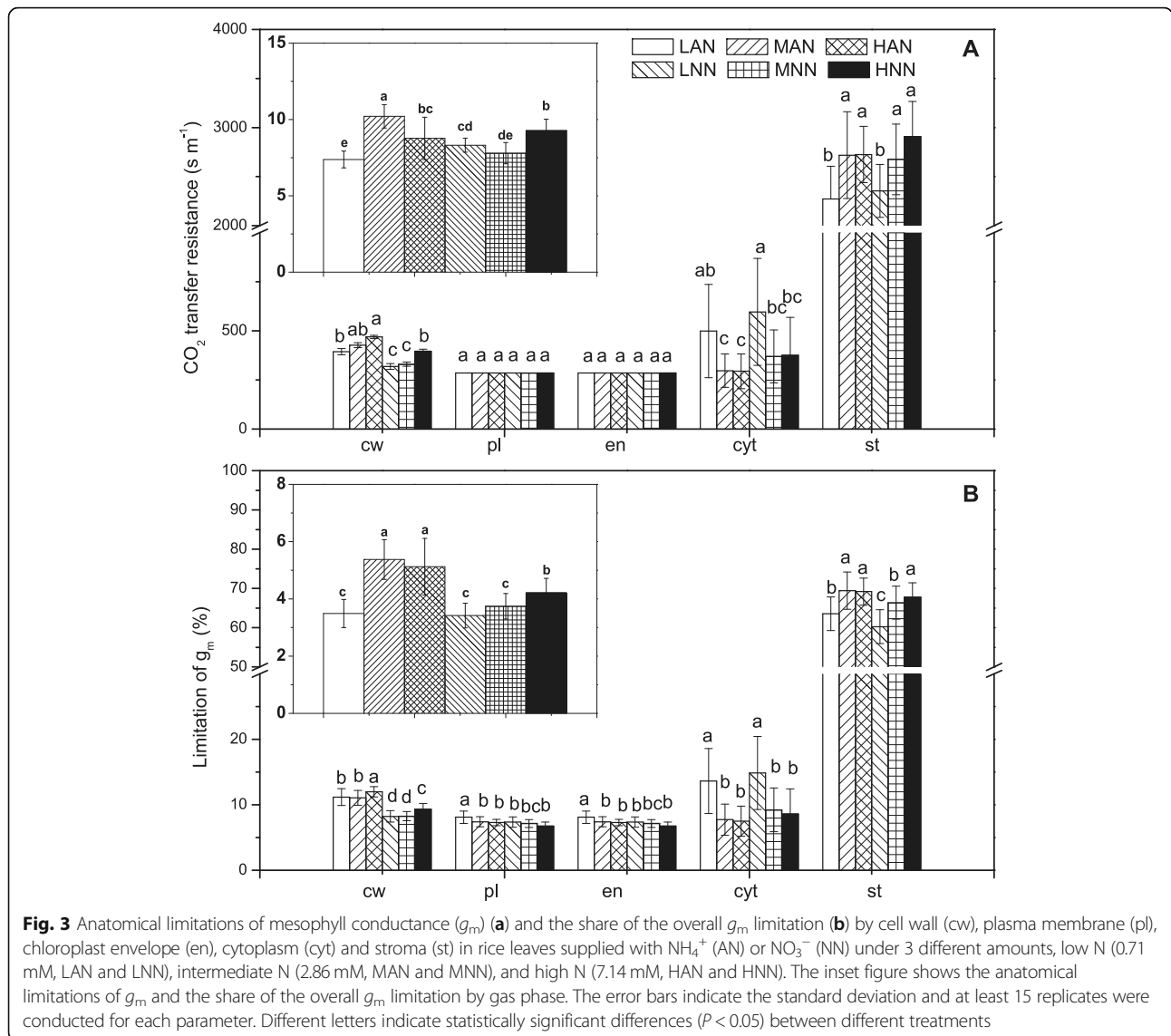
$$C_c - \text{Theoretical (intermediate or high N)}$$
$$= \text{Rubisco (intermediate or high N)}$$
$$\times \frac{C_c}{\text{Rubisco}} \text{(low N)}$$

(3)

As shown in Fig. 5, both theoretical and estimated C_c and/or g_m, as well as the differences between them, increased obviously with increasing leaf N content, and the gap between theoretical and estimated C_c and/or g_m under NH$_4^+$ nutrition was larger than that under NO$_3^-$ nutrition. These results confirmed that the balance between Rubisco content and C_c and/or g_m was weaker when high N and NH$_4^+$ were supplied, and the relatively lower C_c failed to meet the carboxylation demands of

the increased Rubisco content, resulting in decreased PNUE (Fig. 1c, d).

Overall importance of leaf anatomy in determining g_m and PNUE

When leaf nitrogen content was expressed on a leaf dry mass basis, no significant differences in leaf N content between NH$_4^+$ and NO$_3^-$ nutrition were obtained. Therefore, the discrepancies in PNUE between different N forms were primarily caused by the difference in M_A (Fig. 2), which resulted from leaf anatomy characteristics such as leaf density (D_L), leaf thickness (T_L) and cell wall thickness (T_{mc}). In NO$_3^-$-fed plants, the lower M_A was the ultimate result of lower D_L and T_{mc}. However, a lower M_A was not always related to a lower g_m, as observed in the present study; Hassiotou et al. [8] found a negative relationship between M_A and g_m in the range of 100–500 g m^{-2} of M_A, while Hanba et al. [33] clarified a positive relationship in the same range of M_A. These contrasting results were explained by different ways to

Gao *et al. BMC Plant Biology*   (2020) 20:527

Page 6 of 12

Fig. 3 Anatomical limitations of mesophyll conductance (g_m) (**a**) and the share of the overall g_m limitation (**b**) by cell wall (cw), plasma membrane (pl), chloroplast envelope (en), cytoplasm (cyt) and stroma (st) in rice leaves supplied with NH_4^+ (AN) or NO_3^- (NN) under 3 different amounts, low N (0.71 mM, LAN and LNN), intermediate N (2.86 mM, MAN and MNN), and high N (7.14 mM, HAN and HNN). The inset figure shows the anatomical limitations of g_m and the share of the overall g_m limitation by gas phase. The error bars indicate the standard deviation and at least 15 replicates were conducted for each parameter. Different letters indicate statistically significant differences ($P < 0.05$) between different treatments

enhance M_A, as the increases in D_L and T_L were associated with higher g_m, while the opposite conclusion would be obtained if the increase in M_A was a result of a thickened cell wall [8]. Our positive correlation between M_A and g_m implied that the contributions of D_L and/or T_L compensated for the inhibitory effect of T_{mc} on g_m.

To qualify the relative importance of each leaf anatomy trait in explaining g_m, a one-dimensional within-leaf model was calculated to clarify the limitation of g_m in each process [16]. The results showed that more than 90% of the total limitation of g_m came from L_{liq}, which was a consequence of limitation in the cell wall (L_{cw}), plasma membrane (L_{pl}), envelope (L_{en}), cytoplasm (L_{cyt}), and stroma (L_{st}) (Fig. 3) [34]. The decreased contribution of cytoplasmic resistance to g_m under high N resulted from the decreased distance between adjacent chloroplasts, rather than the distance between the cell

wall and chloroplasts [16], and the increase in chloroplast thickness (T_c) extended the transport path for CO_2 from the chloroplast membrane to the carboxylation site in the interior of chloroplasts and resulted in an increasing in r_{st} [35, 36]. Except for the resistance of each part, the chloroplast surface area exposed to intercellular airspace (S_c) was a paramount factor affecting CO_2 liquid resistance (r_{liq}). However, the decreased r_{cyt} and increased S_c partially compensated for the increased r_{st} under high N supply and resulted in an increased g_m, although the effects were weak and did not match the increase in Rubisco content.

Considering the dominant role of S_c in determining g_m, the g_m/Rubisco in Eq. (1) was replaced by the product of g_m/S_c and S_c/Rubisco to demonstrate the effect of leaf anatomies and g_m on PNUE, which can be expressed as follows:
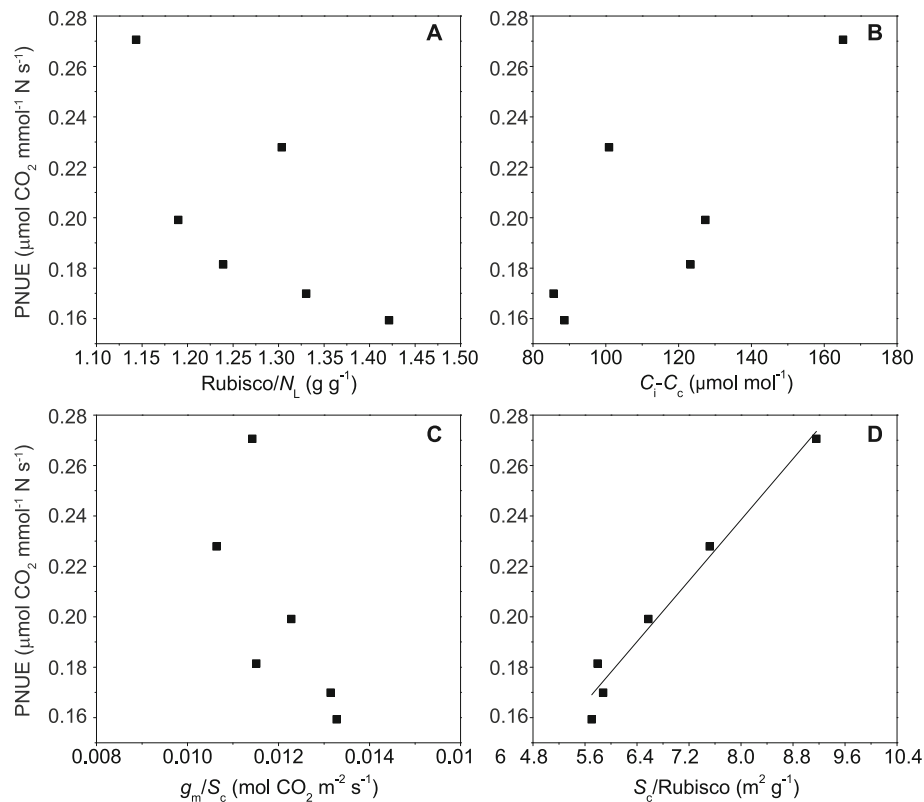
Fig. 4 The relationship between photosynthetic nitrogen use efficiency (PNUE) and the ratio of Rubisco to leaf N content (Rubisco/N_L) (**a**), the difference between intercellular CO_2 concentration and chloroplast CO_2 concentration (C_i-C_c) (**b**), the ratio of mesophyll conductance to chloroplast surface area exposed to intercellular airspace (g_m/S_c) (**c**), and the ratio of chloroplast surface area exposed to intercellular airspace to Rubisco (S_c/Rubisco) (**d**). Data represent the mean of 4 replicates for PNUE, Rubisco, N_L, C_i, C_c, g_m and at least 15 replicates for S_c. The line in the figure represents the following regression equation: y = 0.0299x − 0.0019, R^2 = 0.9700, P < 0.01

$$\text{PNUE} = \frac{g_m}{S_c} \frac{S_c}{\text{Rubisco}} \frac{\text{Rubisco}}{N_L} (C_i - C_c) \qquad (4)$$

According to the formula above and Terashima et al. [37], a positive correlation would be summarized between PNUE and g_m/S_c, which emphasized the potential role of leaf anatomical characteristics except for S_c, as well as the activity of carbonic anhydrase (CA) in contributing to PNUE [37]. However, the weak negative relationship between g_m/S_c and PNUE and the significant positive correlation between the S_c/Rubisco ratio and PNUE suggested the dominant role of S_c in influencing PNUE. Due to the limited knowledge of the relationship between PNUE and the S_c/Rubisco ratio, Onoda et al. [14] did not take this component into consideration when they analyzed the physiological and structural tradeoffs underlying the leaf economics spectrum, and they argued that S_c per Rubisco may not correlate strongly with M_A or PNUE. However, we detected that S_c per Rubisco was a critical parameter associated with PNUE in rice plants supplied with different N nutrition levels. Similar results

were well documented in a review by Terashima et al. [15] and Terashima et al. [37], in which they speculated that, from the perspective of Rubisco and nitrogen use efficiency, thicker leaves with larger S_c were advantageous because the increased ratio of S_c to Rubisco would increase chloroplast CO_2 concentration. The increased S_c/Rubisco ratio in NO_3^-− and high N–fed plants partially resulted from the lower leaf density, which allowed more chloroplast surface area to be exposed to intercellular airspace (Fig. 2a).

Conclusions

In conclusion, we demonstrated that PNUE is decreased in rice plants supplied with high N and ammonium nutrition, which results from unbalanced increases in g_m and Rubisco content. Nitrogen-induced variation in g_m is associated with leaf anatomical traits, especially chloroplast surface area exposed to intercellular airspace (S_c). We further concluded that the S_c/Rubisco ratio is directly related to the response of PNUE to N supply and that its increase is advantageous to the increase in PNUE.
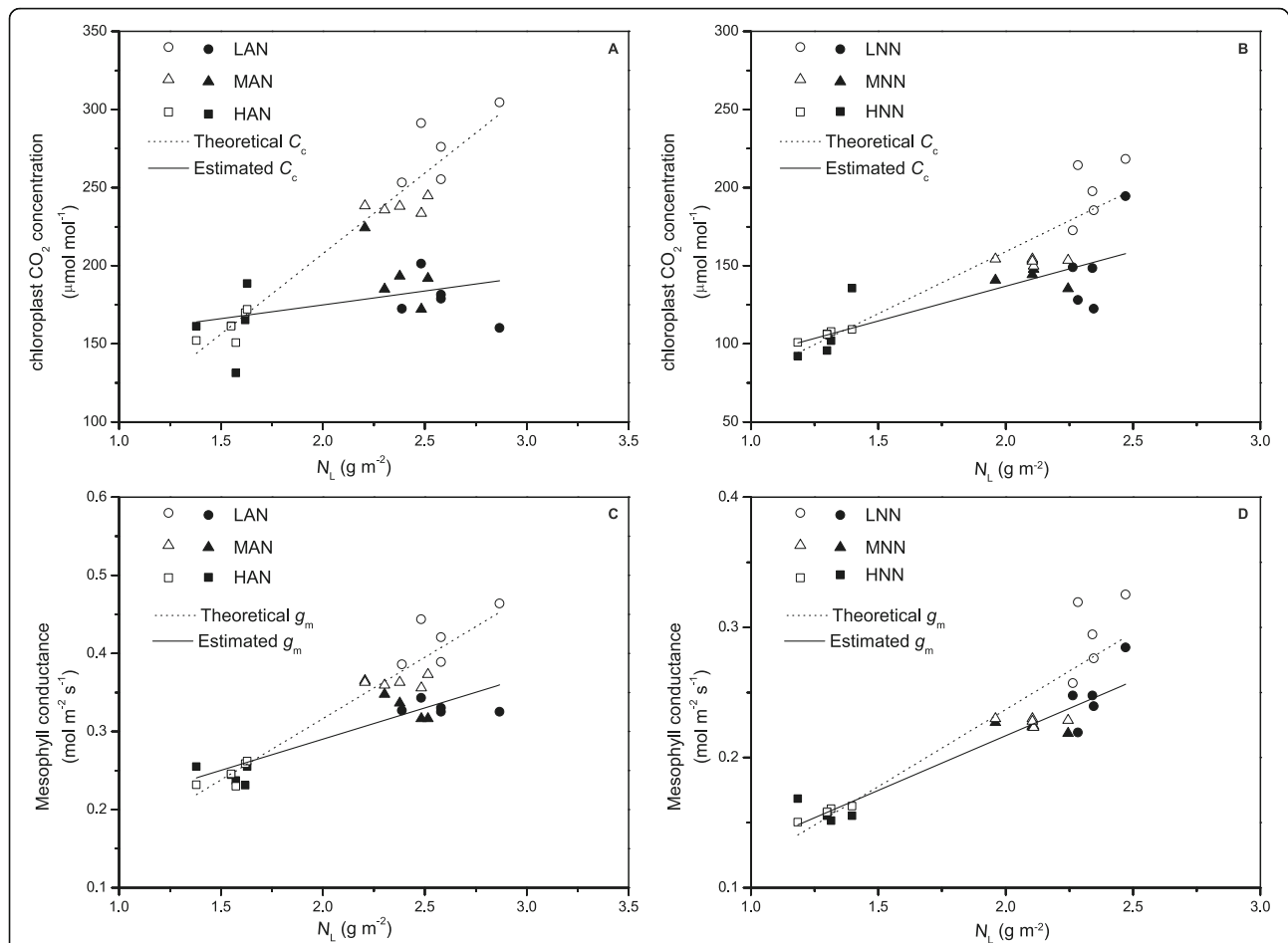
Gao *et al. BMC Plant Biology*   (2020) 20:527

Page 8 of 12

Fig. 5 The relationships between the leaf-N content (N_L) and the estimated and theoretical chloroplast CO_2 concentration (C_c) (**a**, **b**) and the estimated and theoretical mesophyll conductance (g_m) (**c**, **d**) under NH_4^+ (**a**, **c**) and NO_3^- (**b**, **d**) nutrition. Each point represents one replicate (four replicates per treatment). The dashed lines represent the theoretical chloroplast CO_2 concentration and mesophyll conductance, which were calculated according to the ratio of C_c/Rubisco and g_m/Rubisco constant at low-N levels, and the theoretical C_c and g_m at intermediate and high N levels was Rubisco (intermediate or high N) × (C_c/Rubisco or g_m/Rubisco (low N)). The lines represent the estimated C_c and g_m. Rice leaves supplied with NH_4^+ (AN) or NO_3^- (NN) under 3 different amounts, low N (0.71 mM, LAN and LNN), intermediate N (2.86 mM, MAN and MNN), and high N (7.14 mM, HAN and HNN)

Methods

Plant material and growth conditions

Rice seeds (*Oryza sativa* L., ssp. japonica inbred, cv. 'Zhendao 11') were purchased from Mingtian Seed Company (Nanjing, China), disinfected with 10% H_2O_2 for 30 min and germinated in 2.0 mM $CaSO_4$ at 25 °C. The rice seedlings were transferred to 6 L rectangular containers (30 × 20 × 10 cm) when the seedlings developed 2.5 visible leaves, and one quarter-strength mixture of NH_4^+ and NO_3^- nutrient solution (for composition, see below) was supplied. Three days later, the seedlings were transferred to a one half-strength nutrient solution. After 6 days, the seedlings were supplied with full-strength nutrient solution for 1 week, after which the seedlings were supplied with either $(NH_4)_2SO_4$ (AN) or Ca $(NO_3)_2$ (NN) at three different N levels: low N (0.71 mM), intermediate N (2.86

mM), and high N (7.14 mM). Thus, six treatments were applied: LAN (low NH_4^+), MAN (intermediate NH_4^+), HAN (high NH_4^+), LNN (low NO_3^-), MNN (intermediate NO_3^-), and HNN (high NO_3^-). In addition, the macronutrients in the solution were as follows (mM): 0.32 P as KH_2PO_4, 1.02 K as K_2SO_4 and KH_2PO_4 and 1.65 Mg as $MgSO_4$. The micronutrients were (μM) as follows: 35.8 Fe as Fe-EDTA, 9.10 Mn as $MnCl_2 \cdot 4H_2O$, 0.52 Mo as $(NH_4)_6Mo_7O_{24} \cdot 4H_2O$, 18.5 B as H_3BO_3, 0.15 Zn as $ZnSO4 \cdot 7H_2O$, 0.16 Cu as $CuSO_4 \cdot 5H_2O$ and 100 Si as $Na_2SiO_3 \cdot 9H_2O$. $CaCl_2$ was added to the AN, LNN, and MNN solutions to adjust the Ca level to that of the HNN treatment. The nitrification inhibitor dicyandiamide (DCD) was added to each nutrient solution to prevent the oxidation of NH_4^+. The nutrient solutions were changed every 3 days, and the pH was adjusted to 5.50 ± 0.05 each day with 0.1 M HCl or NaOH. All the

treatments were replicated 5 times with a completely randomized design. The temperature in the greenhouse was maintained at 30 °C during the day and 18 °C at night. Light was supplied by SON-TAGRO 400 W bulbs, and the distance between the light and the rice plants was approximately 60 cm. The light intensity was maintained at a minimum of 1000 μmol photons $m^{-2} s^{-1}$ at the leaf level using a 14-h photoperiod.

Measurement of biomass and leaf N content

After all the measurements were completed, plant dry weight was determined after oven-drying at 105 °C for 30 min and then at 70 °C to a constant weight. Pictures of the leaves used for the measurement of P_n were taken with a camera along with a benchmark to calibrate, and the leaf area was obtained by ImageJ Pro Plus, after which the leaves were dried and digested with H_2SO_4-H_2O_2 at 260–270 °C. The leaf N concentration was determined using a digital colorimeter (AutoAnalyzer 3; Bran+Luebbe).

Gas exchange measurements

Twenty days after treatments, a Li–Cor 6400 infrared gas analyzer was used for the simultaneous measurement of light–saturated photosynthesis (P_n) and chlorophyll fluorescence on the newly expanded leaves from 9:00 to 15:00. Leaf temperatures were 25 °C, the relative humidity was 45%, and photosynthetic photon flux density (PPFD) was 1500 μmol $m^{-2} s^{-1}$ for all measurements. After equilibration to a steady state, P_n was recorded and the photosynthetic nitrogen use efficiency (PNUE) was calculated as the ratio of P_n to the leaf nitrogen content per leaf area. The fluorescence (F_s) was also measured simultaneously, and a 0.8 s saturating pulse of light (approx. 8000 μmol $m^{-2} s^{-1}$) was applied to measure the maximum fluorescence (F_m'). The efficiency of photosystem II (Φ_{PSII}) was calculated as $\Phi_{PSII} = 1 - F_s/F_m'$. The total electron transport rate (J_T) was calculated as $J_T = \Phi_{PSII} \times PPFD \times \alpha_{leaf} \times \beta$, where α_{leaf} and β were leaf absorption and the proportion of quanta absorbed by photosystem II, respectively. In this study, α_{leaf} was also assumed to be 0.85, and β was assumed to be 0.5 [38].

The following equations proposed by Harley et al. [24] were used to calculate the CO_2 mesophyll conductance (g_m) and chloroplast CO_2 concentration (C_c):

$$g_m = \frac{P_n}{C_i - \Gamma^* \frac{J_T + 8 \times (P_n + R_d)}{J_T - 4 \times (P_n + R_d)}} \tag{5}$$

$$C_c = C_i - \frac{P_n}{g_m} \tag{6}$$

where C_i is the intercellular CO_2 concentration, Γ^* is the CO_2 compensation point and R_d is the mitochondrial

respiration rate in the light. In the present experiment, Γ^* and R_d were measured on newly expanded leaves according to the method of Li et al. [39]. PPFDs in the cuvette were controlled as the series of 150, 300, and 600 μmol $m^{-2} s^{-1}$. At each PPFD, the ambient CO_2 concentration in the cuvette was adjusted as the series of 25, 50, 75 and 100 μmol CO_2 mol^{-1}. Thirty minutes prior to initiating measurements, leaves were placed in the cuvette with a PPFD of 600 μmol photons $m^{-2} s^{-1}$ and a C_a of 100 μmol CO_2 mol^{-1}.

Anatomical analysis

For the anatomical analysis, approximately 1–2 mm^2 leaf sections were cut and fixed in FAA (95% ethanol: glacial acetic acid: formalin: distilled water = 10:1:2:7), dehydrated in ethanol series, and embedded in paraffin. After cutting into 6 μm transverse sections with a microtome and mounting on glass, the glass was stained with Safranin O and fast green and then mounted in DPX mounting medium. Images of each section were obtained with a light microscope (BX 53, Olympus) with a CCD camera (eXcope X3, DIX, Korea). Leaf thickness (T_L), mesophyll thickness (T_m), leaf density (D_L), and the volume fraction of intercellular air space (f_{ias}) were measured and/or calculated from at least 5 sections from four different leaves, and at least 5 different fields of view were observed for a given section of images. D_L and f_{ias} were calculated as:

$$D_L = \frac{M_A}{T_L} \tag{7}$$

$$f_{ias} = 1 - \frac{\Sigma S_m}{T_m W} \tag{8}$$

where M_A is the specific leaf weight (g m^{-2}), ΣS_m is the total sectional area of mesophyll cells, and W is the width of the section.

For the transmission electron microscope (TEM) analysis, approximately 1–2 mm^2 leaf sections were cut from the middle of newly expanded leaves using two razor blades, fixed in 2.5% glutaraldehyde (0.1 mol L^{-1} phosphate buffer, pH 7.0) and postfixed with 2% osmium tetroxide. Specimens were dehydrated in a graded acetone series and embedded in Epon 812. Ultrathin cross-sections of 90 nm for transmission electron microscopy (TEM) were cut with a Power Tome-XL ultramicrotome, stained with 2% uranyl acetate, and examined with an H-7650 transmission electron microscope. For each sample, 15 cross-sections were chosen to measure mesophyll cell wall thickness (T_{mc}) and total length of the mesophyll cells (L_{mes}) and chloroplasts (L_{ch}) facing the intercellular air space. At least 40 chloroplasts from TEM were observed to measure the chloroplast traits, including chloroplast length (L_c), chloroplast thickness (T_c), chloroplast section area (Sec_c), distance between

two neighbor chloroplasts (ΔL_{chl}), and chloroplast distance from the cell wall (ΔL_{cyt}). The surface area of mesophyll cells to the intercellular air-spaces (S_{mes}), the surface area of chloroplasts exposed to intercellular airspace (S_c), the chloroplast surface area (Sur_c) and volume (Vol_c) were calculated by using the following formula:

$$S_{mes} = \frac{L_{mes}}{W} \, F \tag{9}$$

$$S_c = \frac{L_{ch}}{L_{mes}} S_{mes} \tag{10}$$

where W is the width of the measured section, and F is the curvature correction factor and taken as 1.55 [40].

$$Sur_c = 4 \times \pi \times \left(a \times b^2\right)^{2/3} \tag{11}$$

$$Vol_c = (4/3) \times \pi \times \left(a \times b^2\right) \tag{12}$$

where $a = L_c/2$, and $b = T_c/2$.

The chloroplast number per mesophyll cell (N_c) was determined according to the method of Pyke [41]. Briefly, the leaves were cut into 1–5 mm widths with a scalpel or razor blade, submerged in 3.5% (v/v) glutaraldehyde in a tube and kept in the dark at room temperature for 1 h. The glutaraldehyde solution was then replaced with 0.1 M Na-EDTA (pH 9), and the leaf discs were heat-blocked at 60 °C for 12 h and incubated overnight in the dark at 4 °C. To view chloroplasts in individual cells, a piece of tissue was removed from the tube with fine forceps and placed on a microscope slide in a drop of water. A scalpel handle was used to tap and macerate the tissue fairly vigorously, and a Leica DM2700 M microscope with DIC/Nomarski optics was used to image and count chloroplast numbers with changing focus to avoid duplicate and uncounted chloroplasts (Fig. S3).

The qualification of the anatomical limitations of mesophyll conductance

The one-dimensional gas diffusion model of Tomas et al. [16] was applied in our present study to determine the anatomical limitations of mesophyll conductance, which was given as:

$$g_m = \frac{1}{\dfrac{1}{g_{ias}} + \dfrac{RT_k}{H \cdot g_{liq}}} \tag{13}$$

where g_{ias} and g_{liq} are the gas phase conductance and liquid phase conductance, respectively. R is the gas constant (8.31 Pa m^3 K^{-1} mol^{-1}), T_k is the absolute temperature, and H is Henry's law constant (2943.3 Pa m^3 K^{-1} mol^{-1} for CO_2). The g_{ias}, was calculated as:

$$g_{ias} = \frac{1}{r_{ias}} = \frac{D_a \cdot f_{ias}}{\Delta L_{ias} \cdot \varsigma} \tag{14}$$

where r_{ias} is the resistance of the gas phase to CO_2, D_a is the diffusion coefficient for CO_2 in the gas phase and is set to 1.51×10^{-5} m^2 s^{-1} at 25 °C, f_{ias} is the volume fraction of intercellular air space, ΔL_{ias} was taken as half of the mesophyll thickness, and ς is the diffusion path tortuosity (1.57 m m^{-1}).

The g_{liq} was determined by different components in the cell, including the conductance in the cell wall (g_{cw}), plasma membrane (g_{pl}), cytosol (g_{cyt}), chloroplast envelope (g_{en}), and stroma (g_{st}). Eventually, g_{liq} was calculated as:

$$g_{liq} = \frac{S_c}{\left(r_{cw} + r_{pl} + r_{cyt} + r_{en} + r_{st}\right)} \tag{15}$$

where r_{cw}, r_{pl}, r_{cyt}, r_{en}, r_{st} are the reciprocal terms of g_{cw}, g_{pl}, g_{cyt}, g_{en} and g_{st}, respectively. We used an estimate of 0.0035 m s^{-1} for the g_{pl} and g_{en} as Tomas et al. [16] suggested. In addition, g_{cw}, g_{cyt}, and g_{st} were calculated as:

$$g_i = \frac{1}{r_i} = \frac{r_{f,i} \cdot D_w \cdot p_i}{\Delta L_i} \tag{16}$$

where i stands for cell wall, cytosol, or stroma conductance. $r_{f,i}$ accounted for the reduction in the aqueous phase diffusion coefficient for CO_2 (D_w, 1.79×10^{-9} m^2 s^{-1} at 25 °C) and was taken as 1.0 for cell walls and 0.3 for cytosol and stroma, respectively. p_i was the effective porosity (m^3 m^{-3}) and was taken as 1.0 for the cytosol and stroma and 0.28 for the cell walls. ΔL_i (m) is the diffusion path length in the corresponding component of the diffusion pathway.

The proportion of g_m determined by limited gas-phase conductance (l_{ias}) was calculated as:

$$l_{ias} = \frac{g_m}{g_{ias}} \tag{17}$$

The share of g_m by different components of the cellular phase conductance (l_i) was determined as:

$$l_i = \frac{g_m}{g_i \, S_m} \tag{18}$$

Statistical analysis

One-way ANOVA was applied to assess the differences in each parameter among the treatments with the SPSS 16.0 statistical software package. Significant differences ($P < 0.05$) among treatments are indicated by different letters using the least significant difference test.

Gao *et al. BMC Plant Biology*   (2020) 20:527

Page 11 of 12

Supplementary Information

The online version contains supplementary material available at https://doi.org/10.1186/s12870-020-02731-7.

Additional file 1: Figure S1. Representative light micrographs (A ~ F; scale bar = 200 μm) and transmission electron micrographs (G ~ L; scale bar = 5 μm; M ~ R, scale bar = 1 μm) of rice leaves supplied with NH_4^+ (AN) or NO_3^- (NN) under 3 different amounts, low N (0.71 mM, LAN and LNN), intermediate N (2.86 mM, MAN and MNN), and high N (7.14 mM, HAN and HNN). UEP, upper epidermis; LEP, lower epidermis; V, vascular bundle; CP, chloroplast; CW, cell wall; SG, starch grain; OG, osmiophilic globule. **Figure S2.** The relationship between mesophyll diffusion conductance (g_m) measured with the Harley et al. method and g_m modeled with anatomical parameters (Eq. 13–16). Values are means ± SD of four replicates. The data were fitted by linear regression. Broken lines correspond to the 1:1 relationship. **Figure S3.** Differential interference contrast image of chloroplasts in mesophyll cells separated from leaves. Leaves were cut into small pieces and fixed with 3.5% glutaraldehyde, and the mesophyll cells were individually dispersed on the glass plate and observed by microscopy. The red circles in the figure indicate individual mesophyll cells, and the chloroplast numbers therein were counted; the arrows indicate that the mesophyll cells did not separate efficiently. Bars = 20 μm.

Abbreviations

C_C: Chloroplast CO_2 concentration; C_i: Intercellular CO_2 concentration; D_L: Leaf density; g_m: Mesophyll conductance; g_s: Stomatal conductance; HAN: High NH_4^+; HNN: High NO_3^-; LAN: Low NH_4^+; L_C: Chloroplast length; LNN: Low NO_3^-; M_A: Specific leaf weight; MAN: Intermediate NH_4^+; MNN: Intermediate NO_3^-; N_C: Chloroplasts number per mesophyll cell; N_L: Leaf nitrogen content; P_n: Net photosynthetic rate; PNUE: Photosynthetic nitrogen use efficiency; S_C: Chloroplast surface area facing intercellular air spaces; Sec_C: Chloroplasts section area; S_{mes}: The surface area of mesophyll cells to the intercellular air-spaces; Sur_C: Chloroplast surface area; Vol_C: Chloroplast volume; T_C: Chloroplast thickness; T_L: Leaf thickness; T_m: Mesophyll thickness; T_{mc}: Mesophyll cell wall thickness

Acknowledgements

Not applicable.

Authors' contributions

S.W.G. and L.M.G. conceived and designed the experiments; L.M.G. and K.L.X. performed the experiments; L.M.G. and Z.F.L. analyzed the data and wrote the paper; L.M.G., Z.F.L. and L.D. helped in analysis of the results and manuscript writing; all authors discussed the results and wrote the manuscript. The author(s) read and approved the final manuscript.

Availability of data and materials

The datasets used and analyzed during the current study are available from the corresponding author on reasonable request.

Ethics approval and consent to participate

Not applicable.

Consent for publication

Not applicable.

Competing interests

The authors declare that they have no competing interests.

References

1. Poorter H, Evans JR. Photosynthetic nitrogen-use efficiency of species that differ inherently in specific leaf area. Oecologia. 1998;116:26–37.
2. Bernacchi CJ, Portis AR, Nakano H, von Caemmerer S, Long SP. Temperature response of mesophyll conductance. Implications for the determination of Rubisco enzyme kinetics and for limitations to photosynthesis in vivo. Plant Physiol. 2002;130:1992–8.
3. Zhu XG, De SE, Long SP. Optimizing the distribution of resources between enzymes of carbon metabolism can dramatically increase photosynthetic rate: a numerical simulation using an evolutionary algorithm. Plant Physiol. 2007;145:513–26.
4. Ripullone F, Grassi G, Lauteri M, Borghetti M. Photosynthesis–nitrogen relationships: interpretation of different patterns between *Pseudotsuga menziesii* and *Populus × euroamericana* in a mini-stand experiment. Tree Physiol. 2003;23:137.
5. Li Y, Ren BB, Ding L, Shen QR, Peng SB, Guo SW. Does chloroplast size influence photosynthetic nitrogen use efficiency? PLoS One. 2013;8:e62036.
6. Flexas J, Barbour MM, Brendel O, Cabrera HM, Carriqui M, Diaz-Espejo A, Douthe C, Dreyer E, Ferrio JP, Gago J, et al. Mesophyll diffusion conductance to CO_2: an unappreciated central player in photosynthesis. Plant Sci. 2012;193–194:70–84.
7. Lorimer GH. The carboxylation and oxygenation of Ribulose-1,5-Bisphosphate: the primary events in photosynthesis and photorespiration. Annu Rev Plant Physiol. 2003;32:349–82.
8. Hassiotou F, Ludwig M, Renton M, Veneklaas EJ, Evans JR. Influence of leaf dry mass per area, CO_2, and irradiance on mesophyll conductance in sclerophylls. J Exp Bot. 2009;60:2303–14.
9. Veromann-Jürgenson L-L, Tosens T, Laanisto L, Niinemets Ü. Extremely thick cell walls and low mesophyll conductance: welcome to the world of ancient living! J Exp Bot. 2017;68:1639–53.
10. Veromann-Jürgenson L-L, Brodribb TJ, Niinemets Ü, Tosens T. Pivotal role of mesophyll conductance in shaping photosynthetic performance across 67 structurally diverse gymnosperm species. Int J Plant Sci. 2020;181:116–28.
11. Hassiotou F, Renton M, Ludwig M, Evans JR, Veneklaas EJ. Photosynthesis at an extreme end of the leaf trait spectrum: how does it relate to high leaf dry mass per area and associated structural parameters? J Exp Bot. 2010;61:3015–28.
12. Niinemets U, Wright IJ, Evans JR. Leaf mesophyll diffusion conductance in 35 Australian sclerophylls covering a broad range of foliage structural and physiological variation. J Exp Bot. 2009;60:2433–49.
13. Evans JR, Kaldenhoff R, Genty B, Terashima I. Resistances along the CO_2 diffusion pathway inside leaves. J Exp Bot. 2009;60:2235–48.
14. Onoda Y, Wright IJ, Evans JR, Hikosaka K, Kitajima K, Niinemets Ü, Poorter H, Tosens T, Westoby M. Physiological and structural tradeoffs underlying the leaf economics spectrum. New Phytol. 2017;214:1447–63.
15. Terashima I, Hanba YT, Tazoe Y, Vyas P, Yano S. Irradiance and phenotype: comparative eco-development of sun and shade leaves in relation to photosynthetic CO_2 diffusion. J Exp Bot. 2006;57:343–54.
16. Tomas M, Flexas J, Copolovici L, Galmes J, Hallik L, Medrano H, Ribas-Carbo M, Tosens T, Vislap V, Niinemets U. Importance of leaf anatomy in determining mesophyll diffusion conductance to CO_2 across species: quantitative limitations and scaling up by models. J Exp Bot. 2013;64:2269–81.
17. Carriquí M, Roig-Oliver M, Brodribb TJ, Coopman R, Gill W, Mark K, Niinemets Ü, Perera-Castro AV, Ribas-Carbó M, Sack L, et al. Anatomical constraints to nonstomatal diffusion conductance and photosynthesis in lycophytes and bryophytes. New Phytol. 2019;222:1256–70.
18. Bondada BR, Syvertsen JP. Leaf chlorophyll, net gas exchange and chloroplast ultrastructure in citrus leaves of different nitrogen status. Tree Physiol. 2003;23:553–9.
19. Bondada BR, Syvertsen JP. Concurrent changes in net CO_2 assimilation and chloroplast ultrastructure in nitrogen deficient citrus leaves. Environ Exp Bot. 2005;54:41–8.
20. Poorter H, Niinemets U, Poorter L, Wright IJ, Villar R. Causes and consequences of variation in leaf mass per area (LMA): a meta-analysis. New Phytol. 2009;182:565–88.
21. Golvano M, Felipe M, Cintas A. Influence of nitrogen sources on chloroplast development in wheat seedlings. Physiol Plant. 1982;56:353–60.

22. Raab TK, Terry N. Nitrogen source regulation of growth and photosynthesis in *Beta vulgaris* L. Plant Physiol. 1994;105:1159–66.
23. Antal T, Mattila H, Hakala-Yatkin M, Tyystjarvi T, Tyystjarvi E. Acclimation of photosynthesis to nitrogen deficiency in *Phaseolus vulgaris*. Planta. 2010;232: 887–98.
24. Harley PC, Loreto F, Dimarco G, Sharkey TD. Theoretical considerations when estimating the mesophyll conductance to CO_2 flux by analysis of the response of photosynthesis to CO_2. Plant Physiol. 1992;98:1429–36.
25. Sage RF, Pearcy RW. The nitrogen use efficiency of C3 and C4 plants. Plant Physiol. 1987;84:954–8.
26. Makino A, Nakano H, Mae T. Responses of Ribulose-1,5-bisphosphate carboxylase, cytochrome-F, and sucrose synthesis enzymes in rice leaves to leaf nitrogen and their relationships to photosynthesis. Plant Physiol. 1994; 105:173–9.
27. Ding L, Gao LM, Liu W, Wang M, Gu M, Ren BB, Xu GH, Shen QR, Guo SW. Aquaporin plays an important role in mediating chloroplastic CO_2 concentration under high-N supply in rice (*Oryza sativa* L) plants. Physiol Plant. 2015;156:215–26.
28. Lopes MS, Nogues S, Araus JL. Nitrogen source and water regime effects on barley photosynthesis and isotope signature. Funct Plant Biol. 2004;31:995–1003.
29. Yao BQ, Cao J, Zhao CM, Rengel Z. Influence of ammonium and nitrate supply on growth, nitrate reductase activity and N-use efficiency in a natural hybrid pine and its parents. J Plant Ecol. 2011;4:275–82.
30. Valentine AJ, Osborne BA, Mitchell DT. Form of inorganic nitrogen influences mycorrhizal colonisation and photosynthesis of cucumber. Sci Hortic. 2002;92:229–39.
31. Onoda Y, Hikosaka K, Hirose T. Allocation of nitrogen to cell walls decreases photosynthetic nitrogen-use efficiency. Funct Ecol. 2004;18:419–25.
32. Cheng LL, Fuchigami LH. Rubisco activation state decreases with increasing nitrogen content in apple leaves. J Exp Bot. 2000;51:1687–94.
33. Hanba YT, Miyazawa SI, Terashima I. The influence of leaf thickness on the CO_2 transfer conductance and leaf stable carbon isotope ratio for some evergreen tree species in Japanese warm-temperate forests. Funct Ecol. 1999;13:632–9.
34. Lu ZF, Lu JW, Pan YH, Lu PP, Li XK, Cong RH, Ren T. Anatomical variation of mesophyll conductance under potassium deficiency has a vital role in determining leaf photosynthesis. Plant Cell Environ. 2016;39:2428–39.
35. Terashima I, Miyazawa S-I, Hanba YT. Why are sun leaves thicker than shade leaves? — consideration based on analyses of CO_2 diffusion in the leaf. J Plant Res. 2001;114:93–105.
36. Muller O, Oguchi R, Hirose T, Werger MJ, Hikosaka K. The leaf anatomy of a broad-leaved evergreen allows an increase in leaf nitrogen content in winter. Physiol Plant. 2009;136:299–309.
37. Terashima I, Hanba YT, Tholen D, Niinemets Ü. Leaf functional anatomy in relation to photosynthesis. Plant Physiol. 2011;155:108–16.
38. Manter DK, Kerrigan J. A/C_i curve analysis across a range of woody plant species: influence of regression analysis parameters and mesophyll conductance. J Exp Bot. 2004;55:2581–8.
39. Li Y, Ren BB, Yang XX, Xu GH, Shen QR, Guo SW. Chloroplast downsizing under nitrate nutrition restrained mesophyll conductance and photosynthesis in rice (*Oryza sativa* L.) under drought conditions. Plant Cell Physiol. 2012;53:892–900.
40. Scafaro AP, Von Caemmerer S, Evans JR, Atwell BJ. Temperature response of mesophyll conductance in cultivated and wild *Oryza* species with contrasting mesophyll cell wall thickness. Plant Cell Environ. 2011;34:1999–2008.
41. Pyke K. Analysis of plastid number, size, and distribution in Arabidopsis plants by light and fluorescence microscopy. Methods Mol Biol. 2011; 774:19–32.

Publisher's Note